Available online at www.sciencedirect.com
ScienceDirect
Journal of Power Sources 167 (2007) 420–429
JOURNAL OF POWER SOURCES
www.elsevier.com/locate/jpowsour

An algebraic model on the performance of a direct methanol fuel cell with consideration of methanol crossover

Ken-Ming Yin *

Department of Chemical Engineering and Materials Science, Yuan-Ze University, 135 Yuan-Tung Road, Chung-Li, Taoyuan 32003, Taiwan, ROC

Received 27 December 2006; received in revised form 21 February 2007; accepted 21 February 2007
Available online 27 February 2007

Abstract

An algebraic one-dimensional model on the membrane-electrode-assembly (MEA) of direct methanol fuel cell (DMFC) is proposed. Non-linear regression procedure was imposed on the model to retrieve important parameters: solid polymer electrolyte conductivity κ_m, exchange current density of methanol electro-oxidation at anode catalyst surface $i_{oM,ref}$, and mass diffusivity of methanol in aqueous phase within the porous electrode D_a that correspond to the experimentally measured polarization curves. Although numerical iteration is required for a complete solution, the explicit relationships of methanol concentration, methanol crossover rate, oxygen concentration and cell discharge current density do provide a clear picture of the mass transport and electrochemical kinetics within the various porous media in the MEA. It is shown the cathode mixed potential induced by the parallel reactions of oxygen reduction and oxidation of crossover methanol elucidates the potential drop of the cathode and the decrease of the cell open circuit voltage (OCV). Methanol transport in the membrane is described by the diffusion, electro-osmosis, and pressure induced convection. Detailed accounts of the effects of anode methanol and cathode oxygen feed concentrations on the cell discharge performance are given with correlation to the physical structure and chemical compositions of the catalyst layers (CLs).

Keywords: Direct methanol fuel cell; Membrane-electrode-assembly; Methanol crossover; Mixed potential; Mathematical model

1. Introduction

Direct methanol fuel cell is the recent focus of power sources on portable electronic devices such as laptop computer, cellular phone, and video/audio player, to name a few [1]. Although direct methanol fuel cell (DMFC) has the benefit of small system size and weight, which can be operated at low temperature, it is suffered from the slow electrochemical kinetics of methanol oxidation at the anode and the voltage loss due to methanol crossover through the membrane separator [2–4]. In addition, water management is another crucial issue for a compact design of portable DMFC [5–8]. Wang and co-workers [7,8] indicated that a severe water loss occurs in the anode due to the electro-osmotic drag through the polymer electrolyte membrane, which prohibits the use of concentrated methanol fuel so that additional equipments are required to replenish water in the anode from that in the cathode. Further, the conceived slow oxygen reduction in the cathode could worsen the cell performance in many occasions [9]. Experimental efforts have been carried out to search and formulate more efficient, carbon monoxide resistant anode catalysts [10,11], and to modify the solid polymer electrolyte membrane for a better methanol/water barrier [12,13]. All the materials relevant researches were devoted to the enhancement of single cell performance, and with an eye on a favorable chemical/physical structure of the membrane-electrode-assembly (MEA) [14,15].

Many mathematical models were developed to assist the understanding and improvement of MEA fabrication technique on DMFC [16–29]. A comprehensive account on the current advancement of modeling methods and the associated experimental diagnostic techniques on the polymer electrolyte fuel cells was given by Wang's review article [16], in which a large body of relevant literature was documented. Scott and co-workers [17–21] focused on the mass transport of reactants through the porous electrodes and the interplay with associated electrochemical reactions. Their simulation analyzed

* Tel.: +886 3 4638800x2556; fax: +886 3 4559373.
E-mail address: cekenyin@saturn.yzu.edu.tw.

0378-7753/$ – see front matter © 2007 Elsevier B.V. All rights reserved.
doi:10.1016/j.jpowsour.2007.02.041

Nomenclature

a_a	active area per unit volume in anode catalyst layer (cm^{-1})
a_c	active area per unit volume in cathode catalyst layer (cm^{-1})
A_a	active area per unit mass of PtRu catalyst ($cm^2\ g^{-1}$)
A_c	active area per unit mass of Pt catalyst ($cm^2\ g^{-1}$)
C_b	anode channel concentration of methanol ($mol\ cm^{-3}$)
C_{H^+}	proton concentration in membrane phase ($mol\ cm^{-3}$)
C_M	methanol concentration ($mol\ cm^{-3}$)
$C_{M,ref}$	reference methanol concentration ($mol\ cm^{-3}$)
C_O	oxygen concentration in cathode catalyst layer ($mol\ cm^{-3}$)
C_{Og}	oxygen gas concentration at cathode catalyst layer/gas diffuser ($mol\ cm^{-3}$)
$C_{Og,b}$	cathode channel oxygen gas concentration ($mol\ cm^{-3}$)
$C_{O,ref}$	reference oxygen concentration ($mol\ cm^{-3}$)
C_I^a	methanol concentration in anode catalyst layer at position z_I ($mol\ cm^{-3}$)
C_I^b	methanol concentration in anode backing layer at position z_I ($mol\ cm^{-3}$)
C_{II}^a	methanol concentration in anode catalyst layer at position z_{II} ($mol\ cm^{-3}$)
C_{II}^m	methanol concentration in membrane at position z_{II} ($mol\ cm^{-3}$)
C_{III}^m	methanol concentration in membrane at position z_{III} ($mol\ cm^{-3}$)
D_a	methanol diffusivity in anode catalyst layer ($cm^2\ s^{-1}$)
D_a^{eff}	effective diffusivity of methanol in anode catalyst layer ($cm^2\ s^{-1}$)
D_b	methanol diffusivity in anode backing layer ($cm^2\ s^{-1}$)
D_b^{eff}	effective diffusivity of methanol in anode backing layer ($cm^2\ s^{-1}$)
D_c	oxygen diffusivity in cathode catalyst layer ($cm^2\ s^{-1}$)
D_c^{eff}	effective oxygen diffusivity in cathode catalyst layer ($cm^2\ s^{-1}$)
D_d	oxygen gas diffusivity in cathode gas diffuser ($cm^2\ s^{-1}$)
D_d^{eff}	effective oxygen gas diffusivity in cathode gas diffuser ($cm^2\ s^{-1}$)
D_{H^+}	proton diffusivity in membrane ($cm^2\ s^{-1}$)
D_m	methanol diffusivity in membrane ($cm^2\ s^{-1}$)
F	Faraday constant ($96{,}500\ C\ mol^{-1}$)
$i_{oM,ref}$	reference methanol oxidation exchange current density ($A\ cm^{-2}$)
$i_{oO,ref}$	reference oxygen reduction exchange current density ($A\ cm^{-2}$)
I_{cell}	cell discharge current density ($A\ cm^{-2}$)
I_{leak}	cross-over current density ($A\ cm^{-2}$)
I_O	oxygen reduction current density in cathode catalyst layer ($A\ cm^{-2}$)
j	local transfer current density within catalyst layer ($A\ cm^{-3}$)
k	potential dependent rate constant of methanol oxidation (s^{-1})
k_c	potential dependent rate constant of oxygen reduction (s^{-1})
k_p	permeation constant of pressure induced convection ($cm^2\ s^{-1}\ atm^{-1}$)
K_O	solubility constant of oxygen in liquid phase
K_I	equilibrium constant of methanol between anode backing/anode catalyst layer
K_{II}	equilibrium constant of methanol between anode catalyst layer/membrane
L_a	anode catalyst layer thickness (cm)
L_b	anode backing layer thickness (cm)
L_c	cathode catalyst layer thickness (cm)
L_d	cathode gas diffuser thickness (cm)
L_m	membrane thickness (cm)
m_{Pt}	cathode Pt catalyst loading ($g\ cm^{-2}$)
m_{PtRu}	anode PtRu catalyst loading ($g\ cm^{-2}$)
M_a	molecular weight of O_2 ($g\ mol^{-1}$)
M_b	molecular weight of N_2 ($g\ mol^{-1}$)
M_B	molecular weight of H_2O ($g\ mol^{-1}$)
n_M	electrons transferred of methanol oxidation (=6)
n_O	electrons transferred of oxygen reduction (=4)
N_M	methanol flux ($mol\ cm^{-2}\ s^{-1}$)
P_a	anode pressure (atm)
P_c	cathode pressure (atm)
P_{ca}	critical pressure of O_2 (atm)
P_{cb}	critical pressure of N_2 (atm)
$P_{CO_2,ref}$	reference pressure of CO_2 (=1 atm)
$P_{O_2,ref}$	reference pressure of O_2 (=1 atm)
R	universal gas constant ($8.314\ J\ mol^{-1}\ K^{-1}$)
R_g	universal gas constant ($82.06\ atm\ cm^3\ mol^{-1}\ K^{-1}$)
T	absolute temperature (K)
T_{ca}	critical temperature of O_2 (K)
T_{cb}	critical temperature of N_2 (K)
U_M	reference methanol oxidation open circuit voltage (V)
$U_{M,o}$	standard potential of methanol oxidation (V)
U_O	reference oxygen reduction open circuit voltage (V)
$U_{O,o}$	standard potential of oxygen reduction (V)
V_a	anode electrode potential (V)
V_A	molar volume of O_2 at normal boiling point ($=14.8\ cm^3\ mol^{-1}$)
V_c	cathode electrode potential (V)
V_{cell}	cell voltage (V)

Greek letters

α_a	anodic transfer coefficient of methanol oxidation
α_c	cathodic transfer coefficient of oxygen reduction
ε_a	void fraction in anode catalyst layer
ε_b	void fraction in anode backing layer
ε_c	void fraction in cathode catalyst layer
ε_d	void fraction in cathode gas diffuser
Φ_a	polymer electrolyte potential in anode (V)
Φ_B	association parameter of H_2O (=2.26)
Φ_c	polymer electrolyte potential in cathode (V)
η_a	electrode over-potential in anode (V)
η_c	electrode over-potential in cathode (V)
κ_m	proton conductivity in membrane phase (S cm^{-1})
μ_B	viscosity of water (=1.45 cP)
ρ_C	density of carbon (g cm^{-3})
ρ_{Pt}	density of Pt (g cm^{-3})
ρ_{Ru}	density of Ru (g cm^{-3})
ζ'	electro-osmotic drag coefficient (cm^3 mol^{-1})

individual effects of anode and cathode compartments, and the diffusion coefficient of methanol in the electrode matrix was retrieved in correlation with the experimental data [17,19,20]. Although methanol crossover phenomenon was stressed in their model, an argument of "poisoning effect" on cathode was employed to explain for the cathode voltage drop caused by crossover. That is, active area within the cathode catalyst layer (CL) is blocked by the adsorbed methanol that crossed, and polarization of oxygen reduction is increased due to the less available active area. However, such account was not supported by the physical observations. Wang et al. [30] measured the chemical compositions of cathode effluent of a DMFC and indicated that the crossover methanol is oxidized to CO_2 completely. Ren et al. [31] found the methanol permeation rate is inversely proportional to the membrane thickness at a given cell current density, suggesting the crossover is actually diffusion limited. These experimental findings showed that the over-potential imposed on the methanol oxidation at cathode is large so that methanol is oxidized immediately when reaching the cathode catalyst layer. Further, the intermediate poison species carbon monoxide will not exist at such high overvoltages at the cathode as indicated by the electrocatalytic studies of Dinh et al. [32], which is justified by the theoretical prediction of cathode voltage response in the present work.

Mixed potential concept was adopted on several theoretical modeling of DMFC [4,22–24,26–29]. The methanol crossover causes an internal oxidation current in the cathode catalyst layer, reduces the available cathode potential, and drags a decline of the cell voltage. Elaborate finite difference formulation were used by Zhang and Wang [24] and Guo and Ma [26], which is not computationally efficient and also difficult to be implemented for the in situ data analysis of actual fuel cell system. Wang and Wang [27] did consider the complex two-phase flow in channels using computational fluid dynamics technique; however, both the anode and cathode catalyst layers were simplified as planes of no thickness. Such simplification was later improved by the 3D model of Liu and Wang [28,29], in which the effect of non-linear electrochemical kinetics within the finite catalyst layers was included and detailed water crossover effect was elucidated. The simplified algebraic formulation by Garcia et al. [23] has a neat closed form for the methanol concentration distribution but a linear profile had to be assumed in the anode catalyst layer in their derivation. In view of the non-linear behavior of electrochemical kinetics, such assumption is apparently invalid at the condition of large discharge currents. Guo and Ma's analytical approach [26] included the channel concentration consumption effect; however, a constant concentration was adopted for either methanol or oxygen within the catalyst layer. The purpose of the present study is to device a semi-analytical method that correctly treats the mass transport phenomena occurring in various media of the MEA, as well as the relevant electrochemical kinetics within the active layers. The model includes the methanol crossover effect, which is efficient for the estimation of pertinent MEA kinetic parameters.

2. Mathematical model

A schematic of the membrane-electrode-assembly of DMFC is depicted in Fig. 1. The cathode and anode electrodes are composed of carbon supported catalyst paste that normally brushed onto the respective gas diffuser and backing layers. A complete sandwiched MEA is fabricated by hot-pressing a SPE membrane (for example, Nafion® membrane) in-between the cathode and anode electrodes. Cathode catalyst paste is composed of carbon particle supported platinum catalysts, while that of anode catalyst paste is similarly prepared but with carbon supported platinum/ruthenium alloys. The introduction of ruthenium is to

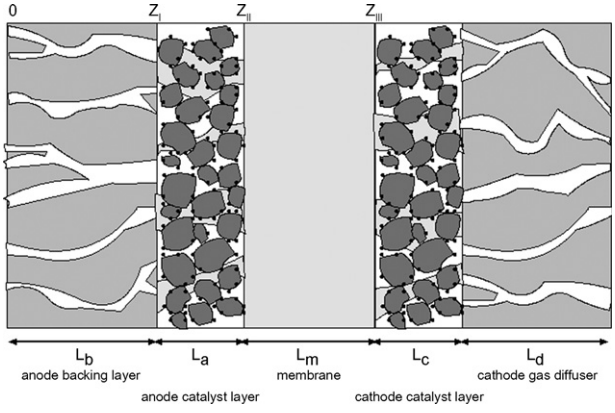

Fig. 1. Schematic of the model region of the membrane-electrode-assembly, not to scale.

Reaction in anode:

$$CH_3OH + H_2O \rightarrow CO_2 + 6H^+ + 6e^-$$

Reactions in cathode:

$$O_2 + 4H^+ + 4e^- \rightarrow 2H_2O$$

$$CH_3OH + H_2O \rightarrow CO_2 + 6H^+ + 6e^-$$

promote de-sorption of the intermediate CO molecule on Pt for the recovery of a free surface for the oxidation of methanol. Both anode and cathode pastes need to be impregnated with recast SPE for an efficient proton transport within the catalyst layers. Cathode or anode diffusion layer is made of either woven carbon cloth or carbon paper for an even distribution of oxygen gas or aqueous methanol.

The modeling region does not include the fluid flow in the channels within the bi-polar plates. Thus, there is no concentration depletion considered in the conduits; only mass transfer resistance in the diffusion layer and the catalyst layer is included. Other assumptions are listed:

(1) The system is isothermal and operated in the steady state condition.
(2) The possible micro-convection and the increased gas void fraction in the anode backing layer, caused by the CO_2 generation in the anode catalyst layer, are not considered explicitly in the model. Nonetheless, the gas bubble effect will be reflected on the estimated effective mass diffusivity of methanol in the porous medium when fitting the model to actual experimental polarization data.
(3) Water is fully flooded in the anode backing layer, anode catalyst layer, membrane, and the cathode catalyst layer, but not in the cathode gas diffuser.
(4) The methanol crossover through membrane is oxidized instantaneously at the membrane/cathode catalyst layer interface due to the large cathode over-potential imposed on the methanol [23,26]. This is justified in the model predictions.
(5) The electronic resistance in carbon matrix is neglected. It should be mentioned that various internal resistances arise due to the different fabrication procedures adopted for the MEA. In addition, extra contact resistance appears when one assembles a single cell. Thus, the membrane conductivity estimated in the present study should be regarded as the total effects from different current conveyers of polymer electrolytes and solid matrix media.
(6) Water crossover and its effect on the variation of methanol concentration are not considered in the present study.

2.1. Mass balance in the anode backing layer

Mass conservation of methanol is

$$\frac{dN_M}{dz} = 0 \tag{1}$$

The diffusive flux of methanol is

$$N_M = -D_b^{eff}\frac{dC_M}{dz} \tag{2}$$

The boundary conditions at $z=0$ and $z=L_b$ are as follows:

$$C_M = C_b \quad \text{at } z = 0 \tag{3}$$

and

$$C_M = C_I^b = K_I C_I^a \quad \text{at } z = L_b \tag{4}$$

It is assumed fast equilibrium preserved at the interface of anode backing layer/anode CL described by Eq. (4) [23,25]. The concentration is

$$C_M = \frac{K_I C_I^a - C_b}{L_b} z + C_b \tag{5}$$

2.2. Methanol conservation in the Nafion® membrane

At steady state, methanol flux in the membrane is constant, which is the resultant of three transport mechanisms: diffusion, electro-osmosis, and pressure induced convection.

$$N_M = -D_m\frac{dC_M}{dz} + \varsigma' C_M\frac{I_{cell}}{F} - k_p C_M\frac{\Delta P}{L_m} \tag{6}$$

The electro-osmotic drag force is proportional to cell current density and local concentration of methanol as suggested by Ren et al. [31]. Darcy type fluid flow is dependent on the pressure difference between cathode and anode as well as the methanol concentration in the membrane [20]. Wang and co-workers [7] analyzed the effect of cathode hydrophobic carbon micro-layer on the hydraulic backing pressure. An extra capillary force prohibited the water crossover and the net water transport coefficient is reduced. Our model can easily be modified to include such feature once the pertinent thermodynamic properties are available for this additional micro-layer. With a linear coordinate transformation $\hat{z} = z - (L_b + L_a)$, C_M can be solved with the prescribed conditions:

$$C_M = C_{II}^m \quad \text{at } \hat{z} = 0 \tag{7}$$

and

$$C_M = C_{III}^m \quad \text{at } \hat{z} = L_m \tag{8}$$

This yields

$$C_M = \frac{(C_{II}^m - C_{III}^m)\exp[-((k_p\Delta P/L_m D_m) - (\varsigma' I_{cell}/D_m F))\hat{z}] + C_{III}^m - C_{II}^m\exp[-((k_p\Delta P/L_m D_m) - (\varsigma' I_{cell}/D_m F))L_m]}{1 - \exp[-((k_p\Delta P/L_m D_m) - (\varsigma' I_{cell}/D_m F))L_m]} \tag{9}$$

The methanol crossover rate is then given

$$N_M = \frac{(C_{III}^m - C_{II}^m)((k_p\Delta P/L_m) - (\varsigma' I_{cell}/F))}{\exp[-((k_p\Delta P/D_m) - (\varsigma' I_{cell}L_m/D_m F))] - 1} - C_{II}^m\left(\frac{k_p\Delta P}{L_m} - \frac{\varsigma' I_{cell}}{F}\right) \tag{10}$$

Eq. (10) is simplified to

$$N_M = \frac{-K_{II}C_{II}^a((k_p\Delta P/L_m) - (\varsigma' I_{cell}/F))}{1 - \exp((k_p\Delta P/D_m) - (\varsigma' I_{cell}L_m/D_m F))} \tag{11}$$

assuming an instantaneous equilibrium between the anode catalyst layer/membrane interface $C_{II}^m = K_{II}C_{II}^a$ [23,25], and an

instant consumption of methanol at the membrane/cathode catalyst layer interface $C^{m}_{III} \approx 0$ [23,26]. The leaking current density caused by the oxidation of crossover methanol is simply

$$I_{leak} = n_M F N_M \tag{12}$$

in which n_M is the number of electron transferred.

2.3. Kinetic expression in the anode catalyst layer

A first order electrochemical reaction on methanol is assumed within the anode catalyst layer:

$$\frac{j}{n_M F} = kC_M \tag{13}$$

where j is the local transfer current density within the anode active layer. The potential dependent rate constant k is defined:

$$k = a_a i_{oM,ref} \frac{1}{n_M F C_{M,ref}} \exp\left(\frac{\alpha_a \eta_a F}{RT}\right) \tag{14}$$

The active area per unit volume is a_a; the exchange current density $i_{oM,ref}$ corresponds to a specified reference concentration $C_{M,ref}$. α_a and η_a are the anodic transfer coefficient and the anode over-potential, respectively. η_a is defined as

$$\eta_a = V_a - \Phi_a - U_M \tag{15}$$

V_a is the anode electrode potential, Φ_a the SPE potential in anode CL, and U_M the open circuit potential (OCP) of methanol oxidation at the reference condition:

$$U_M = U_{M,o} + \frac{RT}{6F} \ln\left(\frac{C^{6}_{H^+} P_{CO_2,ref}}{C_{M,ref}}\right) \tag{16}$$

$U_{M,o}$ is the standard half cell potential of methanol oxidation, $P_{CO_2,ref}$ is chosen 1 atm, $C_{M,ref}$ is set 0.5 mol dm^{-3}, that is, the maximum concentration used in the present study. It should be mentioned that the concentrations used in Eq. (16) should be in mol dm^{-3}. The proton concentration C_{H^+} is available if the SPE conductivity κ_m is known according to the following relationship [33]:

$$\kappa_m = \frac{F^2}{RT} D_{H^+} C_{H^+} \tag{17}$$

2.4. Mass conservation in the anode catalyst layer

Mass conservation is derived for the methanol diffusion with electrochemical reaction:

$$D^{eff}_a \frac{d^2 C_M}{dz^2} - kC_M = 0 \tag{18}$$

Letting $z' = z - L_b$, Eq. (18) is solved

$$C_M = C^a_I \cosh\left(\sqrt{\frac{k}{D^{eff}_a}} z'\right) + \left[\operatorname{cosech}\left(\sqrt{\frac{k}{D^{eff}_a}} L_a\right) C^a_{II} - \coth\left(\sqrt{\frac{k}{D^{eff}_a}} L_a\right) C^a_I\right] \sinh\left(\sqrt{\frac{k}{D^{eff}_a}} z'\right) \tag{19}$$

under the given boundaries:

$$C_M = C^a_I \quad \text{at } z' = 0 \tag{20}$$

and

$$C_M = C^a_{II} \quad \text{at } z' = L_a \tag{21}$$

Since the diffusive flux of methanol at the interface of anode backing layer/anode active layer should be continuous, the flux continuity requirement at $z' = 0$ is used to derive

$$C^a_I = \frac{(D^{eff}_b C_b/L_b) + \sqrt{kD^{eff}_a} \operatorname{cosech}(\sqrt{k/D^{eff}_a} L_a) C^a_{II}}{(D^{eff}_b K_I/L_b) + \sqrt{kD^{eff}_a} \coth(\sqrt{k/D^{eff}_a} L_a)} \tag{22}$$

Another condition required to determine C^a_{II} is the flux continuity constraint at the anode catalyst layer/membrane interface ($z' = L_a$). The final result is

$$C^a_{II} = \frac{\sqrt{kD^{eff}_a}(D^{eff}_b C_b/L_b) \operatorname{cosech}(\sqrt{k/D^{eff}_a} L_a)/((D^{eff}_b K_I/L_b) + \sqrt{kD^{eff}_a} \coth(\sqrt{k/D^{eff}_a} L_a))}{(K_{II}((k_p \Delta P/L_m) - (\varsigma' I_{cell}/F)) \exp[-((k_p \Delta P/D_m) - (\varsigma' I_{cell} L_m/D_m F))])/(1 - \exp[-((k_p \Delta P/D_m) - (\varsigma' I_{cell} L_m/D_m F))]) + (\sqrt{kD^{eff}_a}(D^{eff}_b K_I/L_b) \coth(\sqrt{k/D^{eff}_a} L_a) + kD^{eff}_a)/((D^{eff}_b K_I/L_b) + \sqrt{kD^{eff}_a} \coth(\sqrt{k/D^{eff}_a} L_a))} \tag{23}$$

2.5. Current conservation in the anode catalyst layer

The cell current density is calculated by integration of the local transfer current density across the thickness of anode catalyst layer. That is

$$I_{cell} = \int_0^{L_a} j \, dz' \tag{24}$$

Finally,

$$I_{cell} = n_M F \sqrt{kD^{eff}_a} \left(\coth\left(\sqrt{\frac{k}{D^{eff}_a}} L_a\right) - \operatorname{cosech}\left(\sqrt{\frac{k}{D^{eff}_a}} L_a\right)\right)(C^a_I + C^a_{II}) \tag{25}$$

2.6. Mass conservation of oxygen in the cathode catalyst layer

Mass balance of oxygen is similar to that of methanol in the anode catalyst layer:

$$D_c^{eff}\frac{d^2C_O}{dz^2} - k_c C_O = 0 \tag{26}$$

D_c^{eff} is the effective diffusivity of dissolved oxygen within the cathode catalyst layer, and k_c is the rate constant dependent on the cathode over-potential:

$$k_c = a_c i_{oO,ref}\frac{1}{n_O F C_{O,ref}}\exp\left(\frac{-\alpha_c F\eta_c}{RT}\right) \tag{27}$$

α_c and $i_{oO,ref}$ are the cathodic transfer coefficient and the reference exchange current density, respectively. η_c is defined

$$\eta_c = V_c - \Phi_c - U_O \tag{28}$$

where

$$U_O = U_{O,o} + \frac{RT}{4F}\ln(P_{O_2,ref}C^4_{H^+,ref}) \tag{29}$$

C_O is to be determined with suitable boundary conditions. Let $z'' = z - (L_b + L_a + L_m + L_c)$, the oxygen dissolution at CL/gas diffuser interface is described

$$C_O = \frac{C_{Og}}{K_O} \quad \text{at } z'' = 0 \tag{30}$$

where C_{Og} is the oxygen gas concentration at the interface and K_O is the solubility of oxygen in the flooded cathode catalyst layer. At the membrane/cathode catalyst layer interface, there is no penetration of oxygen into the membrane:

$$\frac{dC_O}{dz''} = 0 \quad \text{at } z'' = -L_c \tag{31}$$

Aqueous oxygen distribution within the cathode catalyst layer is determined

$$C_O = \frac{C_{Og}}{K_O}\cosh\left(\sqrt{\frac{k_c}{D_c^{eff}}}z''\right) \times\left[1+\tanh\left(\sqrt{\frac{k_c}{D_c^{eff}}}L_c\right)\tanh\left(\sqrt{\frac{k_c}{D_c^{eff}}}z''\right)\right] \tag{32}$$

Partial current density contributed from the reduction of oxygen is

$$I_O = n_O F\int_{-L_c}^{0} k_c C_O\,dz'' = n_O F\sqrt{k_c D_c^{eff}}\frac{C_{Og}}{K_O}\tanh\left(\sqrt{\frac{k_c}{D_c^{eff}}}L_c\right) \tag{33}$$

On the other hand, a mass conservation of oxygen in the cathode gas diffuser gives

$$I_O = n_O F\frac{D_d^{eff}}{L_d}(C_{Og,b} - C_{Og}) \tag{34}$$

in which $C_{Og,b}$ is the oxygen gas concentration in the cathode flow channel, D_d^{eff} the effective gas diffusivity in the gas diffuser. Eq. (33) is further simplified to

$$I_O = \frac{n_O F((\sqrt{k_c D_c^{eff}}C_{Og,b})/K_O)\tanh(\sqrt{k_c/D_c^{eff}}L_c)}{1+(\sqrt{k_c D_c^{eff}}L_d/K_O D_d^{eff})\tanh(\sqrt{k_c/D_c^{eff}}L_c)} \tag{35}$$

2.7. Current conservation in the cathode catalyst layer

The resultant current density in the cathode catalyst layer is the difference between the parasitic oxygen reduction current density and oxidation current density of methanol that crossed, or, the leaking current density.

$$I_{cell} = I_O - I_{leak} \tag{36}$$

The cell voltage V_{cell} is calculated by subtracting the activation losses in both anode and cathode (η_a and $|\eta_c|$), and the polymer electrolyte ohmic resistance ($L_m I_{cell}/\kappa_m$) from the theoretical thermodynamic cell voltage ($U_O - U_M$):

$$V_{cell} = U_O - U_M + \eta_c - \eta_a - \frac{L_m I_{cell}}{\kappa_m} \tag{37}$$

2.8. Numerical procedure

Solution procedure is based on the potentiostatic mode, η_a, η_c and I_{cell} are calculated using Newton-Raphson method [34] suggested by Eqs. (25), (36) and (37) for a specified V_{cell}. Numerical derivatives are used to calculate the jacobian matrix element A_{ij}^k at kth iteration [34]. That is,

$$A_{ij}^k = \left.\frac{\partial F_i}{\partial x_j}\right|_{x^k} \approx \frac{F_i(x_l^k(1+\varepsilon\delta_{lj})) - F_i(x_l^k)}{(x_j^k + \varepsilon x_j^k) - x_j^k} \tag{38}$$

F_i represents the non-linear equation i to be solved, while x_j represents η_a, η_c or I_{cell}, δ_{lj} the Kronecker delta, and ε is a step size, 10^{-6} used here.

2.9. Parameter estimation

The model is used to retrieve useful kinetic parameters by non-linear regression with available experimental data. In the present study, D_a, κ_m and $i_{oM,ref}$ are estimated to correlate the experimental polarization curves [23] with the proposed model using Levenberg-Marquardt algorithm [35]. The minimization function is defined

$$F_{min} = \sum_k [I_{exp,k}(E_{exp,k}) - I_{sim,k}(E_{exp,k})]^2 \tag{39}$$

in which the difference of the experimental and simulated cell current densities corresponding to a specified cell voltage is to be minimized in the sum of least squares. Fixed or explicit expressions of thermodynamic, kinetic, and transport parameters used are listed in Table 1 unless otherwise specified. For the case study employed, determination of the anode catalyst layer thickness L_a and the cathode catalyst layer thickness L_c is given as follows. For the anode catalyst loading m_{PtRu} at the 1:1 atomic ratio of PtRu alloy, the weight percentages of Pt and Ru in the alloy

Table 1
Fixed parameters used in the model unless otherwise specified

Parameter	Expression	References
A_a	$52 \times 10^4\ cm^2\ g^{-1}$	[36]
A_c	$52 \times 10^4\ cm^2\ g^{-1}$	Chosen the same as A_a
D_a	$0.5035 \times 10^{-4}\ cm^2\ s^{-1}$	Estimated in the present study
D_a^{eff}	$D_a\varepsilon_a^{1.5}$	[33]
D_b	D_a	Chosen the same as D_a
D_b^{eff}	$D_b\varepsilon_b^{1.5}$	[33]
D_c	$7.4 \times 10^{-8}(\sqrt{\Phi_B M_B}T/V_A^{0.6}\mu_B)$	[38]
D_c^{eff}	$D_c\varepsilon_c^{1.5}$	[33]
D_d	$2.745 \times 10^{-4}/P_c(T/\sqrt{T_{ca}T_{cb}})^{1.823}(P_{ca}P_{cb})^{0.333}(T_{ca}T_{cb})^{0.4167}\sqrt{(1/M_a)+(1/M_b)}$	[39]
D_d^{eff}	$D_d\varepsilon_d^{1.5}$	[33]
D_{H^+}	$1 \times 10^{-4}\ cm^2\ s^{-1}$	[40]
D_m	$4.9 \times 10^{-6}\ \exp(2436((1/333)-(1/T)))$	[18]
$i_{oM,ref}$	$0.7630 \times 10^{-7}\ A\ cm^{-2}$	Estimated in the present study
$i_{oO,ref}$	$0.3189 \times 10^{-7}\ A\ cm^{-2}$	[37]
k_p	$1.17 \times 10^{19}\ \exp(-19098/T)$	[20]
K_I	1.25	[25]
K_{II}	0.8	[23,25]
K_O	$1/R_gT\ \exp(-666/T+14.1)$	[36]
L_b	0.026 cm	Chosen the same as L_d
L_d	0.026 cm	[33]
L_m	0.023 cm	[33]
M_a	$32\ g\ mol^{-1}$	[39]
M_b	$28\ g\ mol^{-1}$	[39]
M_B	$18\ g\ mol^{-1}$	[39]
P_{ca}	49.7 atm	[39]
P_{cb}	33.5 atm	[39]
T_{ca}	154.4 atm	[39]
T_{cb}	126.2 atm	[39]
U_{Mo}	0.03 V	[23]
U_{Oo}	1.23 V	[37]
V_A	$14.8\ cm^3\ mol^{-1}$	[39]
α_a	1	Chosen the same as α_c
α_c	1	[36,37]
κ_m	$0.6842 \times 10^{-1}\ s\ cm^{-1}$	Estimated in the present study
μ_B	1.45 cP	[38]
ζ'	$45\ cm^3\ mol^{-1}$	[31]
ε_c	0.3	[41]
ε_d	0.4	[37]
ε_b	0.4	[37]
ε_a	0.3	[41]
Φ_B	2.26	[38]

are calculated to be 0.659 and 0.341, respectively. For a 40 wt-% PtRu in carbon supported PtRu/C, the thickness of anode catalyst layer is determined

$$L_a = \frac{(0.659 m_{PtRu}/\rho_{Pt}) + (0.341 m_{PtRu}/\rho_{Ru}) + ((1-0.4)m_{PtRu}/0.4\rho_C)}{1-\varepsilon_a} \quad (40)$$

ρ_{Pt}, ρ_{Ru} and ρ_C are the densities of Pt, Ru and carbon. The void fraction in the catalyst layer is denoted ε_a. The active area per unit volume a_a is deduced if the active area per unit mass of PtRu, A_a, is available.

$$a_a = \frac{A_a m_{PtRu}}{L_a} \quad (41)$$

The same argument is applied to the cathode catalyst layer. For a 40 wt-% Pt/C with a loading m_{Pt}, L_c can be determined

$$L_c = \frac{(m_{Pt}/\rho_{Pt}) + ((1-0.4)m_{Pt}/0.4\rho_C)}{1-\varepsilon_c} \quad (42)$$

ε_c is the void fraction in the cathode catalyst layer. The active area per unit volume a_c is expressed

$$a_c = \frac{A_c m_{Pt}}{L_c} \quad (43)$$

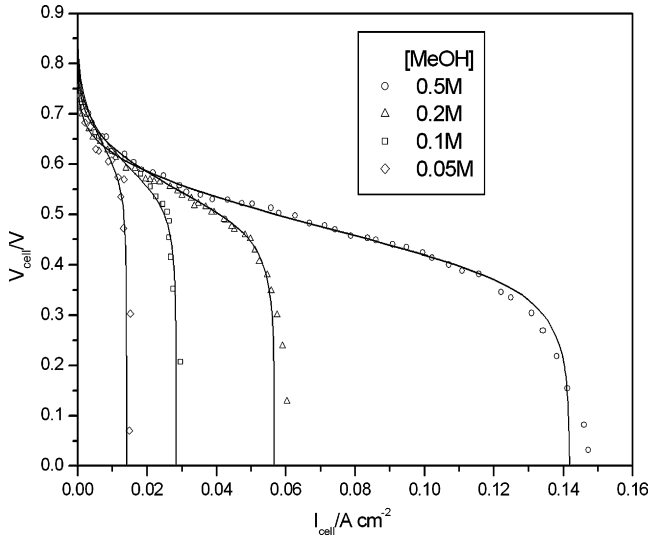

Fig. 2. Comparison of theoretical (lines) and experimental (symbols) polarization curves at different fed methanol concentrations. Experimental data is from Garcia et al. [23]. Anode catalyst: 40% PtRu/C, atomic ratio Pt:Ru = 1:1, PtRu loading: 3 mg cm^{-2}; cathode catalyst: 40% Pt/C, Pt loading: 1 mg cm^{-2} (E-TEK Inc.). Membrane: Nafion® 117. The cell and feed flow temperatures were set 70 °C. Estimated parameters from the model: $i_{oM,ref} = 0.7630 \times 10^{-8}$ A cm^{-2}, $D_a = 0.5035 \times 10^{-4}$ cm^2 s^{-1}, $\kappa_m = 0.6842 \times 10^{-1}$ S cm^{-1}.

3. Results and discussion

The experimental polarization data in Ref. [23] and model predictions in the present study at various fed concentrations of methanol are depicted in Fig. 2. As illustrated in the plot, the limiting behavior occurs much earlier when lower methanol concentration is used, that is, it initiates at larger cell voltages. The theoretical limiting current densities can be calculated simply by setting methanol concentration zero at the anode backing/anode catalyst layer interface, so that

$$I_{\lim} = n_M F D_b^{\text{eff}} \frac{C_b}{L_b} \tag{44}$$

The limiting current densities calculated from Eq. (44) are consistent with the numerically predicted values in Fig. 2 at limiting discharge rates. Note the effects possible micro-convection and gas void within the diffusion layer on the cell discharge, induced by the CO_2 generation, are included implicitly in the estimated diffusivity of methanol in the backing layer D_b (=D_a in Table 1), as discussed in Assumption 2 in Section 2. The predicted discharge curves near the cell open circuit voltage (OCV) exhibits a higher cell voltage when the methanol concentration is lower. This is a consequence of the reduced cathode mixed potential due to the crossover of methanol. Significant voltage loss occurs at the cathode as more methanol crossed due to a higher anode feed concentration. This point will be discussed in more details latter. Fig. 3 shows the decrease of crossover current density with the cell current density. As expected, maximum I_{leak} appears at the open circuit voltage in which mass transfer rate of methanol is the highest. As the cell discharge rate approaches the limiting value, where nearly no concentration of methanol available in the anode catalyst layer, the crossover is diminished accordingly. The corresponding methanol concentrations within the anode catalyst layer and membrane, and oxygen concentration within the cathode catalyst layer are profiled in Fig. 4 at the cell potential 0.5 V. Non-linear concentration profiles appear within the catalyst layers. The discontinuity of methanol concentration at the anode catalyst layer/membrane interface is governed by the phase equilibrium constraint [23,25]. It is shown at the low methanol concentration of 0.05 M limiting behavior emerges as earlier as 0.5 V (also referred to Fig. 2). Oxygen concentration declines rapidly in the cathode catalyst layer. Deepest oxygen penetration path appears at the methanol concentration 0.05 M since lower cell discharge rate allows more residence time for the diffusion of oxidant through the medium.

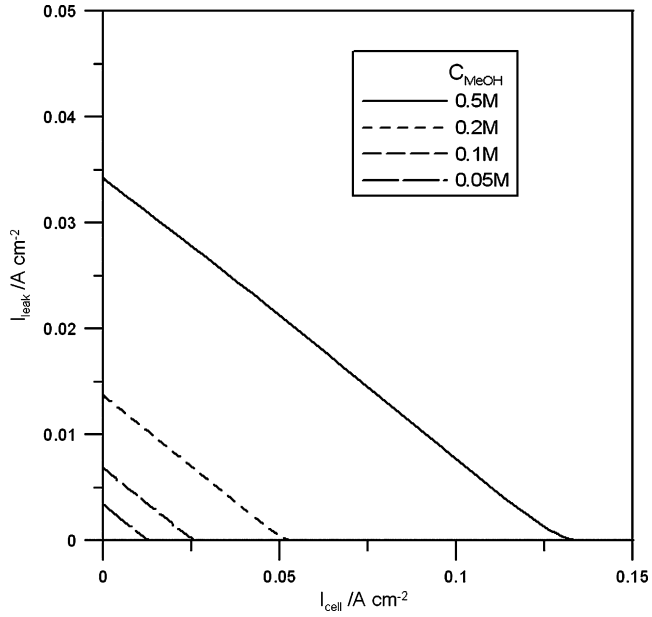

Fig. 3. Leaking (crossover) current density vs. cell current density at various methanol concentrations. Key is the same as in Fig. 2.

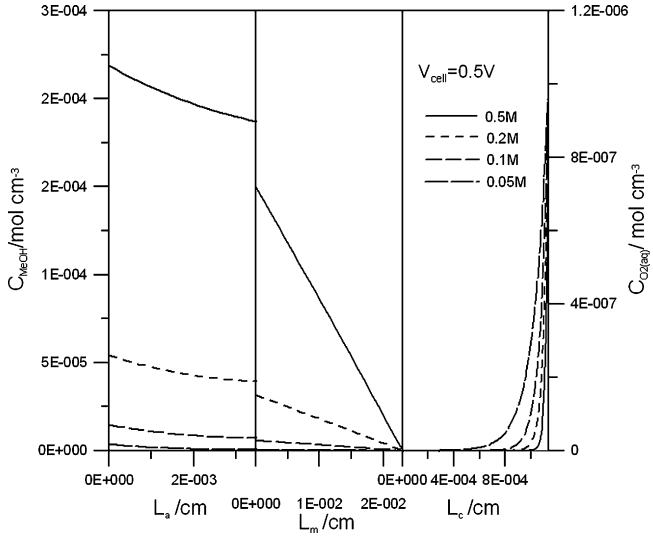

Fig. 4. Simulated methanol concentration profiles within the anode catalyst layer, membrane, and oxygen concentration profiles in the cathode catalyst layer at $V_{cell} = 0.5$ V. Key is the same as in Fig. 2.

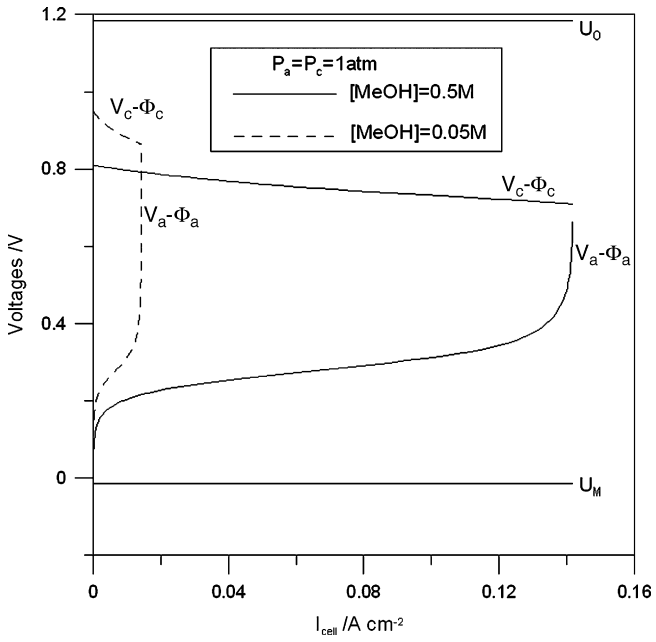

Fig. 5. Anode and cathode potential responses as a function of cell current density at [MeOH] = 0.05 and 0.5 M.

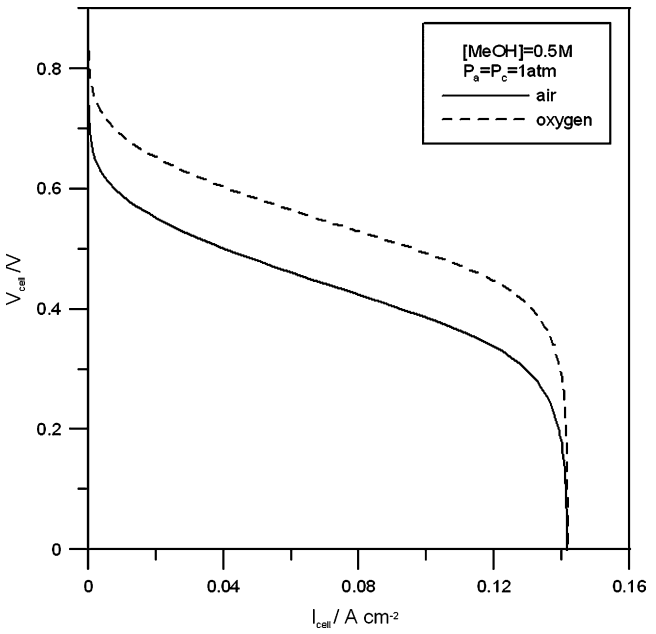

Fig. 6. Effect of oxygen feed composition on the polarization curve.

It is informative to inspect the respective anodic and cathodic potential responses as a function of cell current density, as indicated in Fig. 5. The open circuit potentials of methanol oxidation at anode U_M, and oxygen reduction at cathode U_O are plotted as the references. The cathodic potential, $V_c - \Phi_c$, and the anodic potential, $V_a - \Phi_a$, are displayed respectively. Note the voltage difference between these two is equal to the cell voltage V_{cell} plus the ohmic loss $L_m I_{cell}/\kappa_m$ according to Eq. (45), as derived by the combination of Eqs. (15), (28) and (37):

$$V_{cell} + \frac{L_m I_{cell}}{\kappa_m} = (V_c - \Phi_c) - (V_a - \Phi_a) \quad (45)$$

It is seen the anodic polarization is higher when lower methanol feed concentration (0.05 M) is used, and the anode mass transfer limitation is arrived much earlier than that at high feed concentration (0.5 M). As for the potential characteristics at cathode, higher voltage gain is observed at low than that at high methanol feed as most prominent near the open circuit voltage. This is the consequence of two factors. Firstly, methanol crossover is most severe at low discharge rate and at high anode concentrations as illustrated in Fig. 3. Methanol oxidization at cathode consumes a portion of the cathode oxygen reduction current so as inducing a less available cathode potential that should be otherwise higher. Second, the fact that cell current density limited by the low methanol concentration implies a less requirement of cathode reduction rate. A lower cathode over-potential $|\eta_c|$ is expected as a result. It is also shown in Fig. 5 that the available cathode potential is generally large and sufficient for a complete oxidation of crossed methanol. That is, an instantaneous consumption of the permeated methanol is anticipated.

Fig. 6 depicts the influence of cathode oxygen feed concentration. It is obviously that higher cell OCV and an improved cell discharge behavior are predicted as pure oxygen is used. Mass transfer limitation is still governed by the anode electrochemical reaction whether air or oxygen is fed. The corresponding oxygen concentration profiles in the cathode catalyst layer (not shown) indicate more oxygen is preserved in this layer when oxygen instead of air is fed. On the other hand, methanol concentration depletion is more significant in the anode catalyst layer when oxygen is used.

Fig. 7 illustrates the *I–V* characteristics as the cathode pressure is increased. Higher pressure in the cathode suggests a prohibition of methanol crossover so that a less mixed potential effect is expected. Further, higher oxygen concentration is available for the reduction reaction when cathode is pressur-

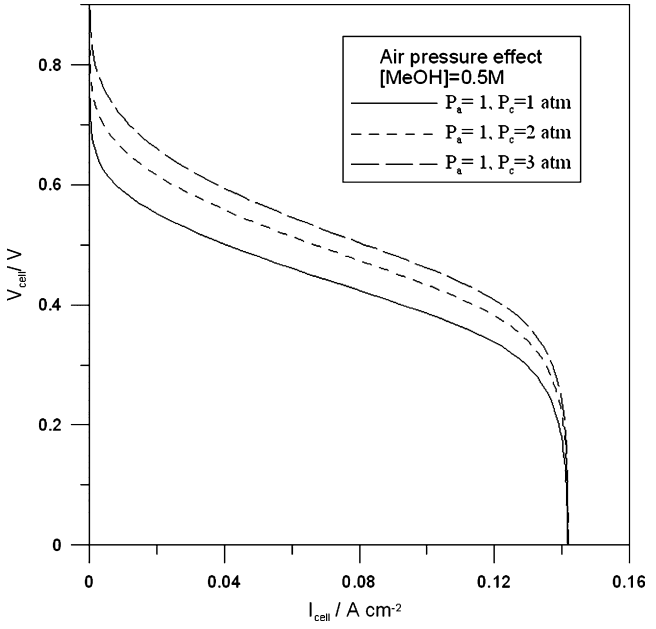

Fig. 7. Cathode air pressure effect on the polarization curve of DMFC.

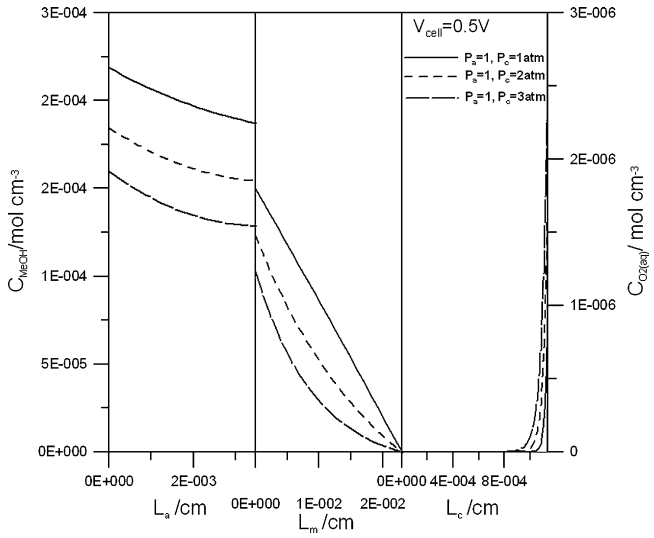

Fig. 8. Concentration profiles of methanol and oxygen within the MEA at $V_{cell} = 0.5$ V, $P_c - P_a = 0$, 1, and 2 atm.

ized. Fig. 8 depicts the detailed concentration distributions at $V_{cell} = 0.5$ V. As expected, higher oxygen concentration is maintained within the cathode catalyst layer with raised cathode pressure. On the other hand, more methanol consumed as more oxygen is available in the cathode. The inhibition of methanol crossover is clear as a significant depressed concentration profile is observed in the membrane phase when the cathode pressure is increased.

4. Conclusion

An algebraic one-dimensional mathematical model on the direct methanol fuel cell is developed. Mass transport of methanol or oxygen through the various media of the membrane-electrode-assembly can be correlated well with the associated non-linear electrochemical kinetics within the catalyst layers. Methanol crossover effect is accounted by the mixed potential theory and justified by the predicted anodic and cathodic potential responses. With the incorporation of a non-linear parameter estimation scheme, this model can be used for a better design on the MEA fabrication of DMFC.

Acknowledgements

The author is indebted to B.L. Garcia for the discussion of several important points in this study. The encouragement from C.C. Chen and C.H. Liang is much appreciated. Their friendship and constant sharing of new ideas are indispensable in many aspects of the research. The research grant received from National Science Council of the Republic of China is acknowledged (NSC 94-2214-E-155-003). Fig. 1 was prepared by W.-K. Yang.

References

[1] J. Larminie, A. Dicks, Fuel Cell Systems Explained, John Wiley & Sons, England, 2003.
[2] Q. Ye, T.S. Zhao, J. Electrochem. Soc. 152 (11) (2005) A2238.
[3] R. Jiang, D. Chu, J. Electrochem. Soc. 151 (1) (2004) A69.
[4] A.A. Kulikovsky, J. Electrochem. Soc. 152 (6) (2005) A1121.
[5] A. Blum, T. Duvdevani, M. Philosoph, N. Rudoy, E. Peled, J. Power Sources 117 (2003) 22.
[6] E. Peled, A. Blum, A. Aharon, M. Philosoph, Y. Lavi, Electrochem. Solid-State Lett. 6 (12) (2003) A268.
[7] G.Q. Lu, F.Q. Liu, C.-Y. Wang, Electrochem. Solid-State Lett. 8 (1) (2005) A1.
[8] F. Liu, G. Lu, C.-Y. Wang, J. Electrochem. Soc. 153 (3) (2006) A543.
[9] J. Ge, H.T. Liu, J. Power Sources 142 (2005) 56.
[10] H. Liu, C. Song, L. Zhang, J. Zhang, H. Wang, D.P. Wilkinson, J. Power Sources 155 (2006) 95.
[11] J.W. Guo, T.S. Zhao, J. Prabhuram, R. Chen, C.W. Wong, Electrochim. Acta 51 (2005) 754.
[12] J. Zhu, R.R. Sattler, A. Garsuch, O. Yepez, P.G. Pickup, Electrochim. Acta 51 (2006) 4052.
[13] Y.-H. Su, Y.-L. Liu, Y.-M. Sun, J.-Y. Lai, M.D. Guiver, Y. Gao, J. Power Sources 155 (2006) 111.
[14] T. Schultz, S. Zhou, K. Sundmacher, Chem. Eng. Technol. 24 (2001) 1223.
[15] W.J. Zhou, W.Z. Li, S.Q. Song, Z.H. Zhou, L.H. Jiang, G.Q. Sun, Q. Xin, K. Poulianitis, S. Kontou, P. Tsiakaras, J. Power Sources 131 (2004) 217.
[16] C.-Y. Wang, Chem. Rev. 104 (2004) 4727.
[17] K. Scott, W.M. Taama, P. Argyropoulos, K. Sundmacher, J. Power Sources 83 (1999) 204.
[18] K. Scott, W.M. Taama, J. Cruickshank, J. Power Sources 65 (1997) 159.
[19] K. Scott, W.M. Taama, J. Cruickshank, J. Appl. Electrochem. 28 (1998) 289.
[20] J. Cruickshank, K. Scott, J. Power Sources 70 (1998) 40.
[21] K. Scott, W.M. Taama, S. Kramer, P. Argyropoulos, K. Sundmacher, Electrochim. Acta 45 (1999) 945.
[22] C.-H. Chen, T.-K. Yeh, J. Power Sources 160 (2006) 1131.
[23] B.L. Garcia, V.A. Sethuraman, J.W. Weidner, R.E. White, R. Dougal, J. Fuel Cell Sci. Technol. 1 (2004) 43.
[24] J. Zhang, Y. Wang, Fuel Cells 4 (2004) 90.
[25] S.F. Baxter, V.S. Battaglia, R.E. White, J. Electrochem. Soc. 146 (2) (1999) 437.
[26] H. Guo, C.-F. Ma, Electrochem. Commun. 6 (2004) 306.
[27] Z.H. Wang, C.Y. Wang, J. Electrochem. Soc. 150 (4) (2003) A508.
[28] W. Liu, C.-Y. Wang, J. Power Sources 164 (2007) 561.
[29] W. Liu, C.-Y. Wang, J. Electrochem. Soc. 154 (3) (2007) B352.
[30] J.T. Wang, S. Wasmus, R.F. Savinell, J. Electrochem. Soc. 143 (1996) 1233.
[31] X. Ren, T.E. Springer, T.A. Zawodzinski, S. Gottesfeld, J. Electrochem. Soc. 147 (2) (2000) 466.
[32] H.N. Dinh, X. Ren, F.H. Garzon, P. Zelenay, S. Gottesfeld, J. Electroanal. Chem. 491 (2000) 222.
[33] D.M. Bernardi, M.W. Verbrugge, AIChE J. 37 (1991) 1151.
[34] B.A. Finlayson, Nonlinear Analysis in Chemical Engineering, McGraw-Hill, 1980.
[35] IMSL Numerical Libraries, Visual Numerics, Houston, 1996.
[36] C. Marr, X. Li, J. Power Sources 77 (1999) 17.
[37] K.-M. Yin, J. Electrochem. Soc. 152 (3) (2005) A583.
[38] J.R. Welty, C.E. Wicks, R.E. Wilson, G. Rorrer, Fundamentals of Momentum, Heat, and Mass Transfer, fourth ed., John Wiley & Sons, 2001.
[39] R.B. Bird, W.E. Stewart, E.N. Lightfoot, Transport Phenomena, Wiley, New York, 1960.
[40] J.S. Newman, Electrochemical Systems, second ed., Prentice-Hall, 1991.
[41] F. Jaouen, G. Lindbergh, G. Sundholm, J. Electrochem. Soc. 149 (2002) A437.